Grip-Pattern Recognition for Smart Guns

J.A. Kauffman, A.M. Bazen, S.H. Gerez, R.N.J. Veldhuis
University of Twente, Department of Electrical Engineering,
Laboratory of Signals and Systems,
P.O. box 217, 7500 AE Enschede, The Netherlands
Phone: +31(0)53 489 2780 Fax: +31 53 489 1060
E-mail: j.a.kauffman@utwente.nl

Abstract— **This paper describes the design, implementation and evaluation of a user-verification system for a smart gun, which is based on grip-pattern recognition. An existing pressure sensor consisting of an array of** 44×44 **piezoresistive elements has been used. An interface has been developed to acquire pressure images from the sensor. The values of the pixels in the pressure-pattern images are used as inputs for a verification algorithm, which is currently implemented in software on a computer. The verification algorithm is based on a likelihood-ratio classifier for Gaussian probability densities. First results indicate that it is possible to use grip-pattern recognition for biometric verification, when allowing a certain false-rejection and false-acceptance rate. However, more measurements are needed to give a more reliable indication of the system's performance.**

Keywords— **biometric verification, likelihood ratio, smart gun, grip-pattern recognition**

I. Introduction

Nowadays there is a growing interest in personalized applications that use biometrics as an access key. Well-known methods use fingerprints, hand geometry, iris scans or voice characteristics to identify a person. Since technology is improving and becoming more affordable, biometrics is becoming more popular for daily use. Powerful processors provide the possibility of doing complex calculations on large sets of data within a short time. This creates new possibilities for high-speed verification or even identification for many everyday applications.

This project has been set up for developing a personalized handgun, a so-called 'smart gun', by making use of biometric verification. The biometric features that will be analyzed are those of the handgrip and squeeze pattern on the gun's butt. The goal is to design a weapon that can only be used by the rightful owner.

The smart-gun concept receives great interest in the US, where weapon safety is an important issue. This technology might prevent many accidents at home where young children get to play with their parent's guns [1] [2]. Also the police (in the US as well as elsewhere) show interest, since carrying a gun in public brings considerable risks. In the US vital statistics show that about 8% of the law enforcement officers, who are killed in a shooting incident, are shot with their own weapon [3].

Fig. 1. Smart gun examples: Saf-T-Block (left), secures the trigger with a code lock. MagLoc Smart Gun (right), works with a magnetic ring which has to be close to the trigger.

Today there are already several types of smart guns available on the market varying from simple trigger locks [4] to more advanced electronically or magnetically controlled systems [5] [6] (Fig. 1). These systems are in general not personalized, because they are controlled by a transmissible magnetic or electronic key. They may also be vulnerable to interference and illegal access with forged keys.

This paper describes the first steps of the development of a personalized smart gun. Section II deals with the design and the implementation of the system's hardware. The algorithm for the biometric verification is discussed in Section III. Subsequently the method for testing the system and the results are explained in Section IV. Finally, the conclusions are presented in Section V.

II. Hardware Design

The design of the smart-gun verification system can be subdivided into separate blocks (Fig. 2): Sensor, Data-Acquisition Module (DAM), Data Processing (DP), Gun Control (GC).

The properties of the sensor will be discussed in Section II-A. The DAM consists of an analog measuring circuit (Section II-B) which is controlled by digital logic (Section II-C). The acquired data is currently transmitted to a PC (DP), which processes the data with a verification algo-

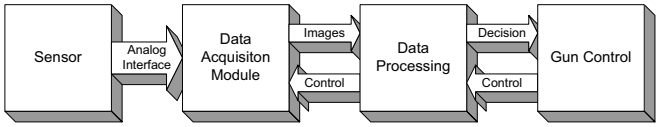

Fig. 2. High-level description of the smart-gun verification system.

Fig. 3. The sensor wrapped around the gun's butt.

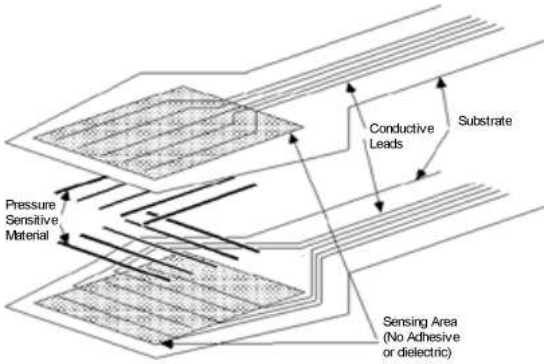

Fig. 4. Sensor schematics model.

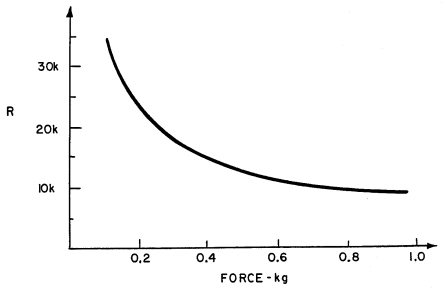

Fig. 5. Force–Resistance characteristic.

rithm (Section III). The Gun Control, responsible for controlling the locking mechanism, has not been implemented yet. The depicted control signals can be used to activate and manage the electronics for power saving purposes.

A. Pressure sensor array

The sensor that is used for this project is a piezo-resistive pressure sensor made by de company Tekscan Inc. [7]. This sensor is available in a size that fits the prototype gun butt, which is that of a *Walther P5* (see Fig. 3).

The sensor consists of two layers of strong and flexible polyester foil. Each layer has 44 silver electrode strips deposited on one side. One layer has vertical strips and the other horizontal. A piezo-resistive ink has been printed on top of the silver leads (Fig. 4).

This construction results in a network of silver strips with a resistive element at each crossing. The resistive elements are sensitive to pressure and have a resistance of more than 5 MΩ at zero load and about 20 kΩ at full load. An example of the pressure-resistance characteristic is shown in Fig. 5 [7].

The entire sensor array can be modelled as a 44×44 network of variable resistors. Fig. 6 shows a similar network of a 4×4 sensor array. In the next section, an explanation is given of how each individual resistance value can be determined.

The Tekscan sensors are available in different sizes and for different pressure ranges ($0-15$kPa to $0-175$MPa or, equivalently, $0-2.2$PSI to $0-25,000$PSI). The sensor used for this project has a range of $0-30$PSI.

B. Resistance measurement

The pressure pattern is measured by determining each resistor value. This is done by subsequently connecting the horizontal and vertical conductors to an analog measuring circuit. The connections can be altered by multiplexers controlled by digital logic.

Fig. 7 shows the schematics [7] for determining the value of resistor element R_{test}, which in this case is R_{13},

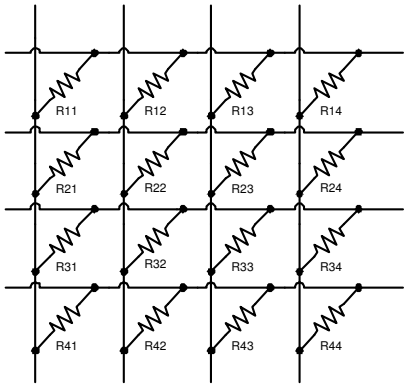

Fig. 6. Schematics model of the pressure sensor array.

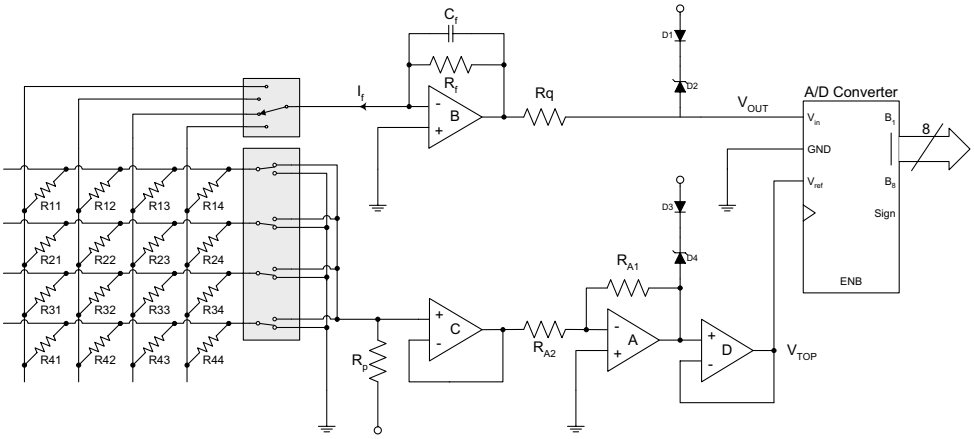

Fig. 7. Schematics for data acquisition (analog part)

using analog components.

Operational amplifier B creates a virtual ground at its negative input. Since all row traces are connected to ground except for the one that is connected to R_{test}, the current that is flowing through this resistor equals I_{f}. Therefore, R_{test} can be calculated if I_{f} and V_{test} are known:

$$R_{\text{test}} = \frac{V_{\text{test}}}{I_{\text{f}}}. \tag{1}$$

Current I_{f} can be measured at the output of OpAmp B (which is equal to V_{OUT}, since V_{in} at the A/D converter is a high-impedance input) and is given by:

$$I_{\text{f}} = \frac{V_{\text{OUT}}}{R_{\text{f}}}. \tag{2}$$

As a result V_{test} will change with the current through the sensor. V_{test} is buffered by OpAmp C, amplified by OpAmp A and buffered again by OpAmp D. The output of OpAmp D, V_{TOP}, is used as the top reference of an ADC. The output ADC_{OUT} is given by:

$$ADC_{\text{out}} = \frac{V_{\text{OUT}}}{\alpha V_{\text{TOP}}} \tag{3}$$

$$= \frac{R_{\text{f}} R_{\text{A2}}}{\alpha R_{\text{A1}}} \frac{1}{R_{\text{test}}}. \tag{4}$$

Capacitor C_{f} makes sure that no high-frequency components from the switching process can pass through and cause damage to the analog to digital converter's (ADC) input. Diodes D1 and D2 are also for protection and make sure that V_{OUT} does not become negative. If they start conducting, resistor R_{q} prevents OpAmp B's output form short circuiting. Resistor R_{p} limits the maximum test current and prevents damage to the components in case of a short circuit in the sensor. The voltage V_{OUT} should always be kept below V_{TOP} for correct results.

C. Multiplexer control and data transport

Digital circuitry is used to control the multiplexers that do the switching for the analog measuring circuit. As shown in the example circuit of Fig. 7, every row needs a 1-to-2 multiplexer for connecting to V_{test} or ground. For the Tekscan (44 $\times$ 44) sensor this means that 44 1-to-2 multiplexers are needed for the row switching. A 1-to-44 multiplexer is needed for the column switching. Since this is not an 'off-the-shelf' component, it is realized by using six 1-to-8 multiplexers of which each can be enabled or disabled. Fig. 8 is a block diagram of how the multiplexers are controlled and how the data are read and sent to the PC.

The 'Address Decoder' is a programmable logic device (PLD) that converts 6-bit column and row addresses to multiplexer control signals. For the columns, it generates an enable signal for one of the six 1-to-8 multiplexers (and disable signals for the 5 others) and a 3-bit address to select one of the 8 switching states. The row address sets one of 44 1-to-2 multiplexers to V_{test} and all others to ground.

The 'Data Control Unit' is another PLD that controls the main functions of the data acquisition module. It executes several actions. First, it generates a column and row address. After a short setup time, it sends a signal to the ADC, which then converts its analog inputs (V_{in} and V_{ref}, Fig. 6) to an 8-bit digital value. This value is read by the 'Data Control Unit' and sent to the serial port of a PC using the RS–232 protocol [8]. An optional USB interface is also included for future experiments that might require a higher bit rate for data transport.

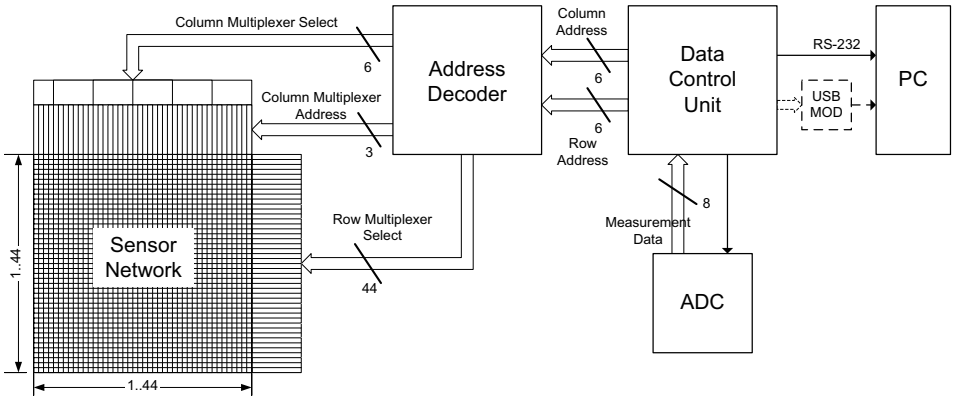

Fig. 8. Digital circuitry for multiplexer control and data transport

III. Algorithm Design

The verification algorithm is based on a likelihood-ratio classifier for Gaussian probability densities [9], [10]. The values of the pixels of the pressure patterns are the features for a verification algorithm. This is based upon the assumption that the pressure pattern will be similar every time the gun is used by the same person.

Measured data can originate form a genuine user or from an impostor. The genuine data is characterized by mean μ_{W} and covariance matrix Σ_{W}, where the subscript $_{\mathrm{W}}$ denotes 'Within-class', while the impostor data is characterized by μ_{T} and Σ_{T}, where the subscript $_{\mathrm{T}}$ denotes 'Total'. Then, the similarity $S(\mathbf{x})$ of a measurement $\mathbf{x}$ to the genuine user, which is derived from the log-likelihood ratio, is calculated by:

$$\begin{aligned} S(\mathbf{x}) &= -(\mathbf{x}-\mu_{\mathrm{W}})^T \Sigma_{\mathrm{W}}^{-1}(\mathbf{x}-\mu_{\mathrm{W}}) \\ &\quad + (\mathbf{x}-\mu_{\mathrm{T}})^T \Sigma_{\mathrm{T}}^{-1}(\mathbf{x}-\mu_{\mathrm{T}}) \end{aligned} \tag{5}$$

If $S(\mathbf{x})$ is above a predetermined threshold, the user is accepted, otherwise he is rejected.

In practice, the means and covariance matrices are unknown and have to be estimated from the data. For our problem, the sensor network has $44 \times 44 = 1936$ nodes, and the feature vector has equally many elements. Therefore, the number of examples needs to be greater than 1936 in order to prevent the covariance matrix from being singular and much greater for a good estimate. Evidently, this large number of measurements would be impractical for user enrollment. Moreover, even if enough measurements would be available, the evaluation of (5) would, with 1936-dimensional feature vectors, still be too high a computational burden.

These problems are solved by orthogonalizing the feature space and at the same time reducing its dimensions. The first step is a principal component analysis (PCA) [11], determining the most important dimensions (with the greatest variance) by doing an eigenanalysis of the covariance matrix. In a PCA the feature-vector space is represented on the orthonormal basis formed by the eigenvectors of its covariance matrix. This also renders it uncorrelated in its dimensions. If the eigenvectors have been sorted according to the corresponding eigenvalues, the dimensions are sorted by their importance. Their number can then be reduced by removing the dimensions with a small or zero contribution to the total variance. Since the training examples of the genuine user are a subset of all samples, the first PCA is based on Σ_{T}. It reduces the feature-vector to N_{PCA} elements.

A further dimension reduction is found by removing the dimensions with the smallest total-to-impostor variance ratios. This is done by means of a linear discriminant analysis (LDA) [11]. First, the transformed feature vectors are multiplied by a square root of the inverse covariance matrix that results after the PCA. This renders the genuine feature vectors uncorrelated with unit variance, but the impostor feature vectors have become correlated again. This is corrected for by a second PCA based on the new Σ_{T}. Since the PCA involves a unitary transform, this does not change Σ_{W} which is identity. LDA now amounts to selecting the $N_{\mathrm{LDA}} \leq N_{\mathrm{PCA}}$ dimensions corresponding to the largest eigenvalues of the final (diagonal) impostor covariance matrix Λ_{T}.

The sequence of transformations described above can be replaced by one multiplication by an $N_{\mathrm{LDA}} \times 1936$ matrix, denoted by $\mathbf{V}$. Let $\nu_{\mathrm{W}} = \mathbf{V}\mu_{\mathrm{W}}$ and $\nu_{\mathrm{T}} = \mathbf{V}\mu_{\mathrm{T}}$ denote the transformed means, and let $\mathbf{y} = \mathbf{V}\mathbf{x}$ denote the transformed input feature vectors, then (5) reduces to:

$$S(\mathbf{y}) = -(\mathbf{y}-\nu_{\mathrm{W}})^T(\mathbf{y}-\nu_{\mathrm{W}}) + (\mathbf{y}-\nu_{\mathrm{T}})^T\Lambda_{\mathrm{T}}^{-1}(\mathbf{y}-\nu_{\mathrm{T}}) \quad (6)$$

Because Λ_{T} is a diagonal matrix of much smaller dimensions than the original covariances matrices, the number of computations has decreased considerably.

IV. Experimental Results

As described in Section III a decision is made by comparing the matching score (6) to a threshold T. If $s(\mathbf{y}) > T$, then the user is accepted, else he is rejected. Before the effects of the choice for T on the performance can be assessed, the parameters N_{PCA} and N_{LDA} have to be set. Their optimal values have been found experimentally by determining the system's *equal error rate* (EER) for different combinations of N_{PCA} and N_{LDA}.

A. Method

For the experiment a collection of 900 handgrip patterns was gathered from a group of 30 mostly untrained subjects. From each subject 30 right-hand grip images were taken. Between every three measurements the subject was asked to completely renew his grip by releasing the gun and retaking it. The three measurements for same grip register variations in the pressure while holding the same grip, since it is quite impossible to maintain a constant (within the DAM's precision) grip-pressure distribution. The renewal of the grip is necessary to register variations in the grip.

The experiment was repeated three times for different training and test sets: for every subject the measurements were split by taking: (1) the first 10 for testing and the remaining 20 for training, (2) the second 10 for testing and the remaining 20 for training, (3) the third 10 for testing and the remaining 20 for training. The results of the three experiments were averaged.

The covariance matrix for the first PCA of the GC was estimated from the entire training set. Due to the small number of measurements available per subject, the estimation for the LDA of the covariance matrices of the LC was expected to become very poor. To solve this problem one covariance matrix was estimated for all local classes by averaging all 30 local covariance-matrix estimates. This is based upon the assumption, that the covariance matrices of the local classes are similar across different subjects.

B. Results

Both the training and test sets were used to determine the average EER for different combinations of N_{PCA} and N_{LDA}. The results are displayed as contour plots in Figs. 9 and 10.

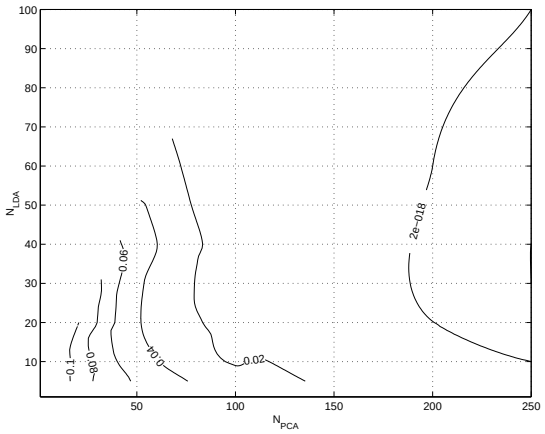

Fig. 9. Contour plot of the EER for different values of N_{PCA} and N_{LDA} for experiments with the training set.

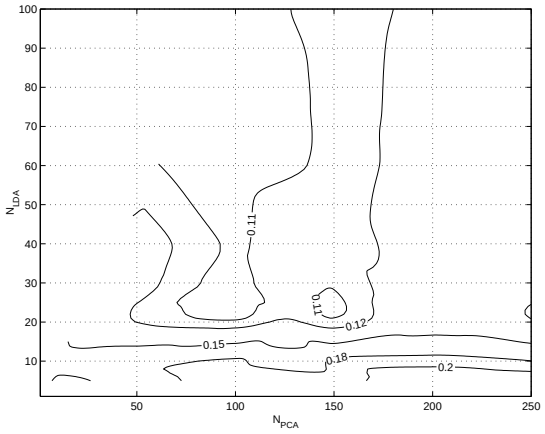

Fig. 10. Contour plot of the EER for different values of N_{PCA} and N_{LDA} for experiments with the test set.

The contour plot of Fig. 9 shows that the EER quickly drops for $N_{\mathrm{PCA}} > 100$ and $N_{\mathrm{LDA}} > 10$. This is not surprising, since the more characteristic features that are used the better the system can distinguish individual images. At a certain point the system gets *overtrained* and becomes more sensitive for the individual (per image) characteristics than for subject class characteristics. This becomes clear when looking at the contour plot of the test set in Fig. 10. It shows that there is an optimum for the EER for $N_{\mathrm{PCA}} = 100$ and $N_{\mathrm{LDA}} > 25$. The small optimum at $N_{\mathrm{PCA}} = 150$ and $N_{\mathrm{LDA}} = 25$ is likely to be a statistical contingence, due to the small data set.

It is best to choose N_{LDA} as low as possible to limit the number of resources for the system. Therefore, the parameters of the current implementation are set to $N_{\mathrm{PCA}} = 100$ and $N_{\mathrm{LDA}} = 30$. Fig. 11 shows the the FAR and the FRR (for the training and test sets) for this setting as func-

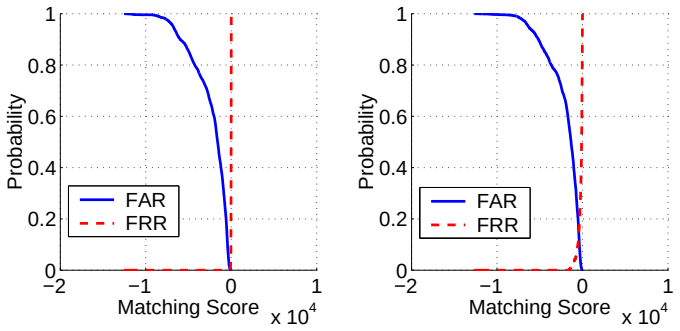

Fig. 11. FAR and the FRR for different matching scores. Left: training set, right: test set.

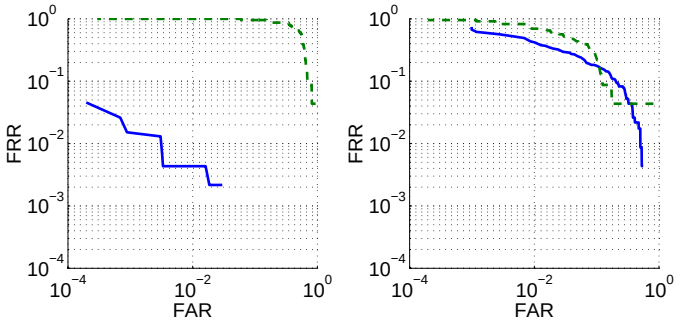

Fig. 12. ROCs for the training (left) and test (right) sets. The dashed line is the ROC for a Euclidean classifier without dimension reduction.

tions of the matching-score threshold T. The corresponding receiver operation characteristics (ROC) are displayed in Fig. 12. The dashed lines, which are the ROCs for a Euclidean distance classifier, show that the results cannot be considered very precise: the EER for the test set is below that for the training set. The opposite would be expected.

The results demonstrate that the handgrip pressure pattern contains information that can be used for verification. Results appear to improve if PCA is used to transform and reduce the feature-vector space. It was also found that the second reduction step by LDA to N_{LDA} features does not (to a limited level) significantly affect the EER.

The current values for the ROC are not precise enough to make a well-founded statement about the performance of the system. To improve these results, more data are needed from a greater population and with more scans per subject. Probably another important aspect, that determines the outcome's precision, is the lack of shooting experience of the subjects. It appeared that more experienced subjects (who had handled the gun more often and over a longer period) showed better results than first-time subjects. The three most-experienced subjects even showed an FAR and FRR of 0% with this limited number of tests. To approximate realistic situations, the data should be collected from experienced subjects at a shooting range.

V. Conclusions

The current hardware implementation has proven to be useful for the first experiments and demonstrations within this project. The piezo-resistive sensor array of the Tekscan sensor has been found suitable for detecting handgrip squeeze patterns and appeared to be a good option for a low-cost experimental setup. The current system uses a PC for the implementation of the verification algorithm. Though the training of the system requires some extensive computations, the verification part is quite straightforward and suitable for an efficient hardware implementation.

The test results demonstrate that the pressure pattern contains information that can be used for verification. The results for the test set show that the EER is optimal for $N_{\text{PCA}} = 100$ and $N_{\text{LDA}} > 25$. To save system resources, like memory and logic components, it is best to set N_{LDA} low. The current values for the ROC are not precise enough to make a well-founded statement about the performance of the system. This is caused by the limited number of data that was collected for training and testing.

References

[1] Donna L. Hoyert., Elizabeth Arias, Betty L. Smith, Sherry L. Murphy, and Kenneth D. Kochanek. National Vital Statistics Reports. Volume 49 Number 8, NVSS, September 21 2001.

[2] Anonymous. Factsheet: Firearm Injury and Death in the United States. Technical report, Johns Hopkins University; Center for Gun Policy and Research, 2000.

[3] The national Uniform Crime Reporting Program. Law Enforcement Officers Killed and Assaulted. Technical report, Federal Bureau of Investigation, 2001.

[4] Concept Development Corporation. Saf-t-block. Web Page, Januari 2003. `http://members.aol.com/saftblok/`.

[5] Smart Lock Technology Inc. Magloc. Web Page, Januari 2003. `http://www.smartlock.com/`.

[6] Peter Wetzig. The World's First Totally Electronic Hand Gun. *Metal Storm Limited*, April 2000. `http://www.metalstorm.com/12_odwyervle/smartgun.html`.

[7] William L. Maness et al. Pressure and contact sensor for measuring dental occlusion. United States Patent; 4,856,993, Aug. 1989. Tekscan, Inc.

[8] Craig Peacock. Interfacing the rs–232 port. Web Page, August 2001. `http://www.beyondlogic.org/serial/serial1.htm`.

[9] H.L. Van Trees. *Detection, estimation, and modulation theory*. Wiley, New York, 1968.

[10] Asker M. Bazen and Raymond N.J. Veldhuis. Likelihood Ratio-Based Biometric Verification. *Proceedings of ProRISC 2002*, 2002.

[11] Richard O. Duda and Peter E. Hart and David G. Stork. *Pattern Classification (2nd Edition)*. Wiley-Interscience, 2000.